

# Six-fold coordinated carbon dioxide VI

VALENTIN IOTA\*, CHOONG-SHIK YOO\*, JAE-HYUN KLEPEIS, ZSOLT JENEI, WILLIAM EVANS AND HYUNCHAE CYNN

Lawrence Livermore National Laboratory, Livermore, California 94551, USA

\*e-mail: iota1@llnl.gov; yoo1@llnl.gov

Published online: 10 December 2006; doi:10.1038/nmat1800

Under standard conditions, carbon dioxide ( $\text{CO}_2$ ) is a simple molecular gas and an important atmospheric constituent, whereas silicon dioxide ( $\text{SiO}_2$ ) is a covalent solid, and one of the fundamental minerals of the planet. The remarkable dissimilarity between these two group IV oxides is diminished at higher pressures and temperatures as  $\text{CO}_2$  transforms to a series of solid phases, from simple molecular to a fully covalent extended-solid V, structurally analogous to  $\text{SiO}_2$  tridymite. Here, we present the discovery of an extended-solid phase of  $\text{CO}_2$ : a six-fold coordinated stishovite-like phase VI, obtained by isothermal compression of associated  $\text{CO}_2$ -II (refs 1,2) above 50 GPa at 530–650 K. Together with the previously reported  $\text{CO}_2$ -V (refs 3–5) and a-carbonia<sup>6</sup>, this extended phase indicates a fundamental similarity between  $\text{CO}_2$  (a prototypical molecular solid) and  $\text{SiO}_2$  (one of Earth's fundamental building blocks). We present a phase diagram with a limited stability domain for molecular  $\text{CO}_2$ -I, and suggest that the conversion to extended-network solids above 40–50 GPa occurs via intermediate phases II (refs 1,2), III (refs 7,8) and IV (refs 9,10). The crystal structure of phase VI suggests strong disorder along the  $c$  axis in stishovite-like  $P4_2/mnm$ , with carbon atoms manifesting an average six-fold coordination within the framework of  $sp^3$  hybridization.

Carbon dioxide is a prototypical molecular system, with strong covalent bonds within the  $\text{O}=\text{C}=\text{O}$  molecules and rather weak quadrupolar interactions between them. At high pressures and temperatures,  $\text{CO}_2$  transforms to a series of solid polymorphs with differing intermolecular interactions, chemical bonding and crystal structures (Fig. 1). Phase V, in particular, consists of a network of corner-sharing  $\text{CO}_4$  tetrahedra, structurally similar to  $\text{SiO}_2$  tridymite. Thus,  $\text{CO}_2$ -V is a fundamentally new material that exhibits extremely low compressibility<sup>5</sup> and strong optical nonlinearity<sup>3</sup>. The large disparity in chemical bonding between the extended network and molecular  $\text{CO}_2$  results in a broad metastability domain for phase V, to room temperature and almost to ambient pressure<sup>3,5</sup>.

The other  $\text{CO}_2$  phases, II (refs 1,2), III (refs 7,8) and IV (refs 9–11) (formed in the intermediate pressure–temperature regime) exhibit strong intermolecular interactions, enhanced substantially over those of typical quadrupolar molecular solids<sup>12</sup>. The strong interactions lead to enhanced collective behaviour of molecules, and result in strong associations of neighbouring molecules in phase II, strain-induced disorder in phase III and molecular bending in phase IV. Accordingly, these phases have been considered as intermediates between the simple molecular phase I and the fully extended phase V.

The crystallographic similarities between  $\text{CO}_2$  and  $\text{SiO}_2$  polymorphs<sup>2,5,10,13</sup> suggest the existence of other  $\text{CO}_2$  extended solids, including six-fold stishovite. The strong covalence in C–O

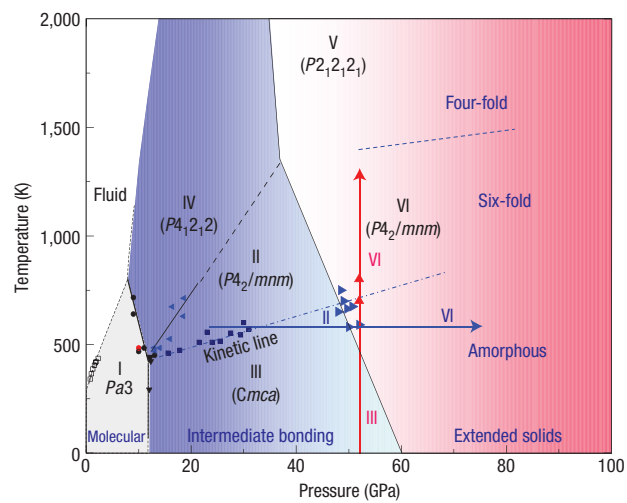


**Figure 1** Phase diagram of carbon dioxide illustrating the molecular to non-molecular phase transitions to four- and six-fold coordinated carbon atoms. The arrows represent two typical experimental paths: isothermal compression of phase II to 90 GPa or isobaric heating of phase III to 1,200 K, shown together with the observed phase transformations. Phase V was synthesized by laser heating the quenched phase VI well above  $\sim 1,500$  K (marked as a dashed line). The dash-dot line between phases II and III indicates a kinetic line, whereas the broken melting line of phase IV was not measured. The grey, blue and red colours, respectively, signify the stability fields of molecular, intermediate and extended phases and the electron delocalization occurring gradually in  $\text{CO}_2$ , via the intermediate phases II and IV.

bonds and the rigidity of  $sp^3$ -bond angles, however, seem to hamper the formation of six-fold coordinated carbon units<sup>14</sup>. Total-energy calculations predict four-fold cristoballite<sup>14</sup> and/or layered carbonate<sup>4</sup> structures to be among the most stable configurations, whereas six-fold  $\text{CO}_2$  are thought to stabilize only at ultrahigh pressures above 400 GPa (ref. 15).

Here, we report the discovery of fully extended stishovite-like  $\text{CO}_2$  phase VI, formed at pressures below 100 GPa (Fig. 1). On the basis of a large number of resistive- and laser-heating experiments using membrane diamond-anvil cells (mDACs), we propose the relationship between the molecular and extended phases in the pressure–temperature domain shown in Fig. 1.

$\text{CO}_2$ -VI is stabilized by isothermal compression of phase II to pressures above 50 GPa at temperatures 530–650 K. As shown in

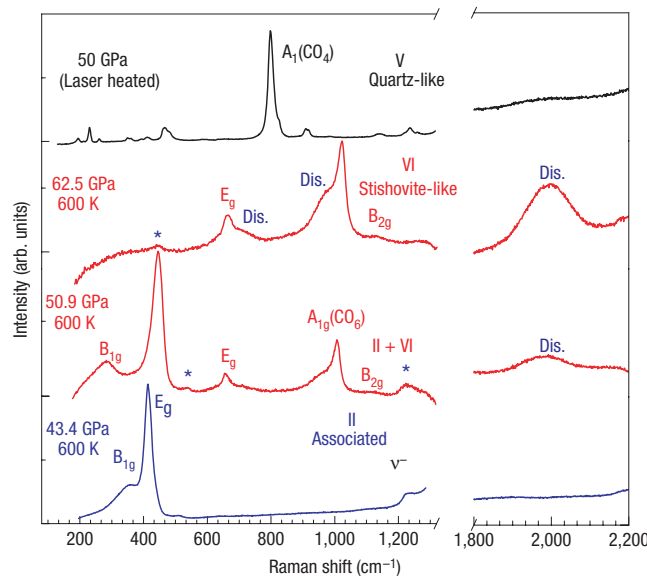


**Figure 2** Raman spectra of carbon dioxide phases at high temperatures and pressures, representing the phase transition from strongly associated phase II to fully extended, stishovite-like phase VI at 600 K and 51 GPa. Note that residual phase II (marked by an asterisk) still apparent at this pressure gradually weakens and eventually disappears above  $\sim$ 65 GPa, whereas the features of phase VI are enhanced. CO<sub>2</sub>-VI is quenchable at ambient temperature, and laser heating the quenched phase VI to above 1,500 K transforms it to CO<sub>2</sub>-V. The peaks labelled ‘Dis.’ are assigned to disorder within the stishovite structure as described in text.

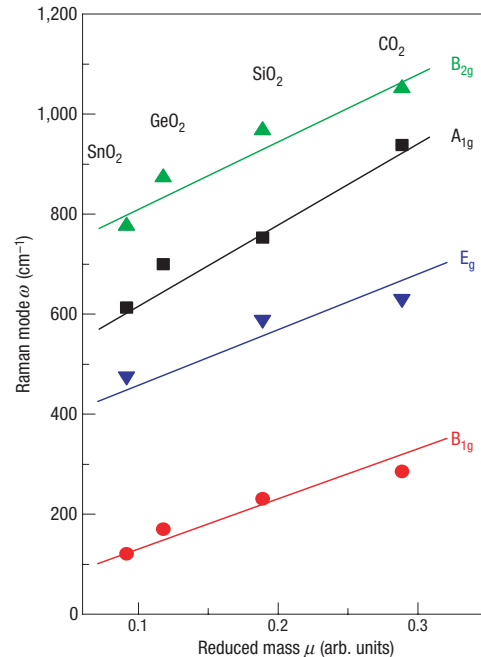


**Figure 3** Raman mode frequencies of CO<sub>2</sub>-VI compared with those of other group IV dioxides in rutile structures. We find a near-linear scaling of the four principal Raman bands with the reduced mass, strongly supporting our stishovite-like assignment for phase VI.

**Table 1** Comparison of the major Raman frequencies observed in extended CO<sub>2</sub> phases and corresponding SiO<sub>2</sub> polymorphs in four- and six-fold configurations. The numbers indicate the Raman shift in cm<sup>-1</sup> at ambient pressure, obtained by extrapolation from Fig. 4 for CO<sub>2</sub> phases and from ref. 16 for SiO<sub>2</sub> phases.

Four-fold		Six-fold	
SiO <sub>2</sub>	CO <sub>2</sub> -V	SiO <sub>2</sub>	CO <sub>2</sub> -VI
464	660	967	1,051
206	285	753	905
128	240	589	620
		231	285

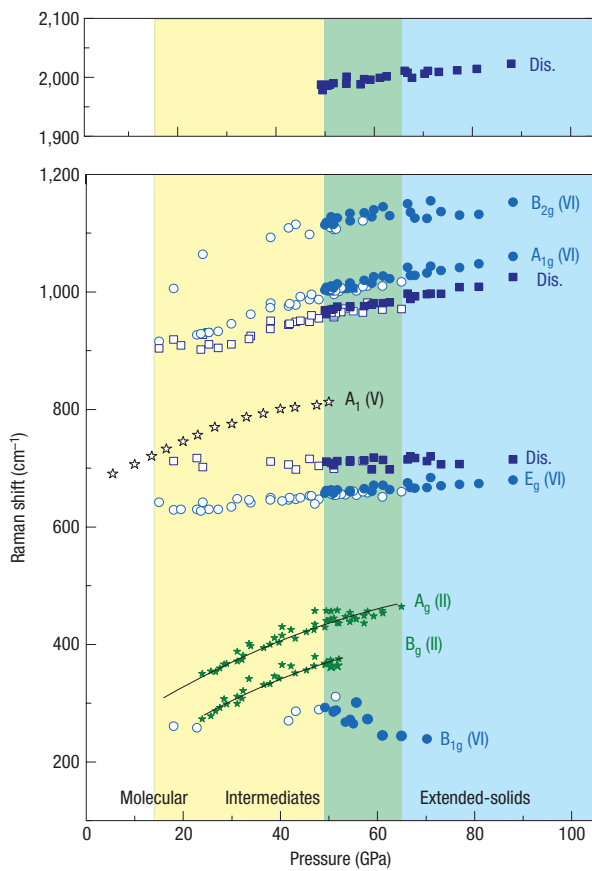
Fig. 2, the most notable Raman feature of CO<sub>2</sub>-VI is the emergence of a strong band around 1,010 cm<sup>-1</sup> at 50 GPa. This mode frequency is substantially higher than that of four-fold coordinated carbon in CO<sub>2</sub>-V ( $\sim$ 800 cm<sup>-1</sup>) (ref. 3), indicating that it probably originates from six-fold coordinated carbons in octahedral sites—similar to the A<sub>1g</sub> mode of stishovite<sup>16</sup>. Following this assignment, we further associate the peaks at 300 cm<sup>-1</sup> to B<sub>1g</sub>, 680 cm<sup>-1</sup> for E<sub>g</sub>, and a weak, but measurable band at 1,100 cm<sup>-1</sup> to B<sub>2g</sub>, thus accounting for all four Raman-active modes reported in stishovite<sup>16</sup>. Importantly, the frequencies of these modes scale very well to those observed in SiO<sub>2</sub> polymorphs (see Table 1). In addition, in Fig. 3 we compare the observed Raman spectra of CO<sub>2</sub>-VI with those of other group IV dioxides in rutile structures. We find that the frequencies of all four Raman-active modes scale linearly with the reduced mass, strongly supporting the present assignment of phase VI as stishovite-like. The data for SiO<sub>2</sub>, GeO<sub>2</sub> and SnO<sub>2</sub> are from previous studies<sup>17</sup>.

Figure 4 summarizes the pressure dependence of the Raman modes of the new material. In addition to the four modes assigned

to the stishovite-like structure, we observe a number of broad Raman features in CO<sub>2</sub>-VI, centred at  $\sim$ 2,000, 950 and 700 cm<sup>-1</sup> at 65 GPa, which we assign to disorder in the stishovite structure. In fact, the 950 and 700 cm<sup>-1</sup> Raman bands are very similar to those of amorphous CO<sub>2</sub> (ref. 6). Although the 2,000 cm<sup>-1</sup> band is well within the overtone range of the A<sub>1g</sub> band, we note that the C–O stretching mode of carbosonium<sup>18</sup> or a theoretically suggested ring dimer<sup>19</sup> also appear in this frequency range.

The II-to-VI transition is strongly affected by kinetics, requiring slow compression over several hours in a wide pressure range. Although the conversion to CO<sub>2</sub>-VI starts at  $\sim$ 50 GPa (530 K), residual CO<sub>2</sub>-II is observable to 60–65 GPa. In this pressure range, the A<sub>1g</sub> mode of phase VI gradually increases, whereas the E<sub>g</sub> mode of phase II gradually decreases in intensity and eventually disappears above 60–65 GPa, as shown in Fig. 2. CO<sub>2</sub>-VI can also be produced by isobaric heating of phase III to  $\sim$ 700–900 K above 50 GPa, although this method typically leads to a less crystalline phase. Once CO<sub>2</sub>-VI is formed at high pressures and temperatures, it remains stable in a wide pressure range, from 90 GPa (the maximum pressure applied in the present study), down to 20 GPa, below which it transforms back to phase II. CO<sub>2</sub>-VI is also stable in a wide temperature range from ambient to at least 1,200 K at 50 GPa, the maximum temperature reached in our resistive heating experiments. Further heating CO<sub>2</sub>-VI to above 1,500 K using a Nd:YLF laser converts the sample to CO<sub>2</sub>-V (Fig. 2).

The stability of six-fold coordinated carbon dioxide at around 50 GPa is remarkable. It has not been reported in any other carbon compounds, and theory has predicted its existence only at substantially higher pressures above 400 GPa at 0 K (ref. 15). We attribute its low-pressure stability to the crystal structure of phase II (ref. 2) in which each carbon atom already has six quasi-nearest-neighbour oxygen atoms, facilitating the formation of the six-fold C–O single-bond configuration observed in phase VI. In fact, our



**Figure 4** Pressure-dependence of the Raman modes observed in the extended phases of  $\text{CO}_2$ -VI (in blue) and V (in black from ref. 3), overlaid with those of  $\text{CO}_2$ -II (in green) for comparison. The broad features arising from the disorder in phase VI are also shown (in dark blue, labelled as 'Dis'). Open and filled symbols signify the data obtained during pressure upstroke and downstroke, respectively.

X-ray diffraction data confirm the close similarity between the crystal structures of phases II and VI (Fig. 5).

Figure 5 shows the X-ray diffraction data of phases II and VI obtained at elevating pressures at 600 K. Phase II diffraction pattern is well described in terms of stishovite-like  $P4_2/mnm$ ;  $a = 3.5430(5)$  Å,  $c = 4.1544(7)$  Å, C:2a(0,0,0) and O:2f( $x, x, 0$ ) $x = 0.247(1)$ . Small differences observed in the 110 and 101 reflections represent a minor, less than 0.1%, lattice distortion in the  $ab$  plane<sup>2</sup>.

Figure 5 shows a remarkable similarity between the diffraction patterns of phases II and VI, confirming the structural similarity between the two phases. Indeed, the diffraction patterns of phase VI are reasonably well refined in terms of the same space group  $P4_2/mnm$ ;  $a = 3.4284(3)\{3.363(1)$  Å,  $c = 4.0259(7)\{3.973(4)$  Å at 59{70} GPa. Furthermore, all observed pressure-induced diffraction changes occur smoothly and continuously across the phase transition. The two most characteristic changes are a gradual diminution of the 002/111 intensity ratio and an overall broadening of all reflection lines. However, in  $P4_2/mnm$ , carbon atoms in the 2(a) sites can contribute only to the  $hkl$  reflections matching  $h + k + l = 2n$ , whereas oxygen atoms in the 4(f) do not have any additional reflection conditions. Therefore, to describe the observed diffraction changes in phase VI, it is necessary to introduce the movement of atomic positions away from the  $ab$  plane, by either allowing carbon atoms to deviate from 2a(0, 0, 0)

along the  $c$  axis to 4e(0, 0,  $z$ ) (shown in Fig. 5b) or oxygen atoms from 4f( $xx0$ ) to 8m( $xxz$ ) or more generally 16k( $xyz$ ) (not shown), reducing the atomic occupancy correspondingly. In this model, we found that the value of the displacement  $z$  increases gradually above 50 GPa, approaching  $z = 0.095\{0.170\}$  at 59{70} GPa (see Supplementary Information, Fig. S1 inset). This results in all carbon atoms well within carbon–oxygen single-bond distances, 1.45–1.71 Å, having six quasi-nearest oxygen atoms in a highly distorted octahedral configuration as illustrated in Fig. 5b.

Alternatively, the observed diffraction changes may also be described in terms of large-amplitude thermal vibrations. The best refinements of the X-ray data in Fig. 5a, however, result in relatively large thermal displacement parameters;  $0.16(1)\{0.110(8)\}$  Å<sup>2</sup> for carbon and  $0.11(1)\{0.096(8)\}$  Å<sup>2</sup> for oxygen at 59{70} GPa, two–three times those previously obtained in phase II at similar temperatures. Therefore, we prefer the static-disorder model described above, with the fixed initial displacement parameters at  $0.058$  Å<sup>2</sup> for both C and O. Nevertheless, we found that the latter refined thermal displacement parameters become larger again;  $0.109(8)$  Å at 59 GPa and  $0.115(7)$  Å at 70 GPa or actual thermal motion of  $\sim 0.33$ – $0.34$  Å. These values are quite comparable to the displacement of carbon atoms along the  $c$  axis,  $0.4$ – $0.6$  Å (see Fig. 5b). In this regard, it is difficult to differentiate the static disorder from the dynamic thermal model. In either case, carbon atoms remain on average six-fold coordinated with oxygen atoms.

Although the present X-ray data confirms the stishovite-like  $P4_2/mnm$  structure for phase VI, there is a subtle difference from stishovite. That is, the  $\text{CO}_6$  octahedron in phase VI is made of two edge-sharing  $\text{CO}_4$  units that share a single carbon atom. Nevertheless, the similarity in the Raman spectra between phase VI and stishovite clearly indicates that up to 90 GPa the amount of disorder is relatively small to maintain an average coordination of six. The short interatomic oxygen–oxygen contact distance in the  $ab$  plane of phase II, 2.1–2.4 Å depending on the pressure–temperature conditions, is well in the repulsion regime and thus leads to mechanical instability<sup>14,20</sup> and the observed structural frustration on pressure increase. This results in a configuration of carbon atoms manifesting six-fold coordination while maintaining the frame work of  $sp^3$  hybridization at elevated pressures.

We point out that the proposed disordered  $P4_2/mnm$  model cannot be uniquely determined based on the limited number of reflections observed in the present powder X-ray diffraction patterns. Nevertheless, in addition to its close similarity to the parent phase II, the present model is consistent with all of our other experimental observations. First, it explains the increased ionicity of C–O bonds in phase VI, as observed in the Raman spectra and also predicted by theory<sup>15</sup>. Second, it accounts for the significant temperature dependence of the specific volume of phase VI (see Supplementary Information, Fig. S1). At 70 GPa, the specific volume of phase VI is  $0.305 \text{ cm}^3 \text{ g}^{-1}$  at 600 K but collapses to  $\sim 0.290$ – $0.220 \text{ cm}^3 \text{ g}^{-1}$  at 300 K, well within the range of fully extended solids (for example,  $0.265 \text{ cm}^3 \text{ g}^{-1}$  for phase V at 300 K)<sup>5</sup>. Third, the proposed structural disorder is consistent with the emergence of the broad Raman bands in phase VI (marked as 'Dis' in Figs 2 and 4). Finally, it provides a mechanism for the stability of phase VI at moderate pressures and temperatures (above 50 GPa and 550 K), in contrast to the extreme pressures (400 GPa) predicted by theory<sup>15</sup>.

Finally, considering the rich abundance of carbon, oxygen and silicon in the Earth's mantle, the new high-density form of six-fold carbon dioxide may offer new concepts in geo- and mineral chemistry. For example,  $\text{CO}_2$  could exist in the Earth's mantle as four- and six-fold covalent solids and within alloys or solid solutions with  $\text{SiO}_2$  and/or other minerals. The structural similarities between  $\text{CO}_2$  and  $\text{SiO}_2$  polymorphs would

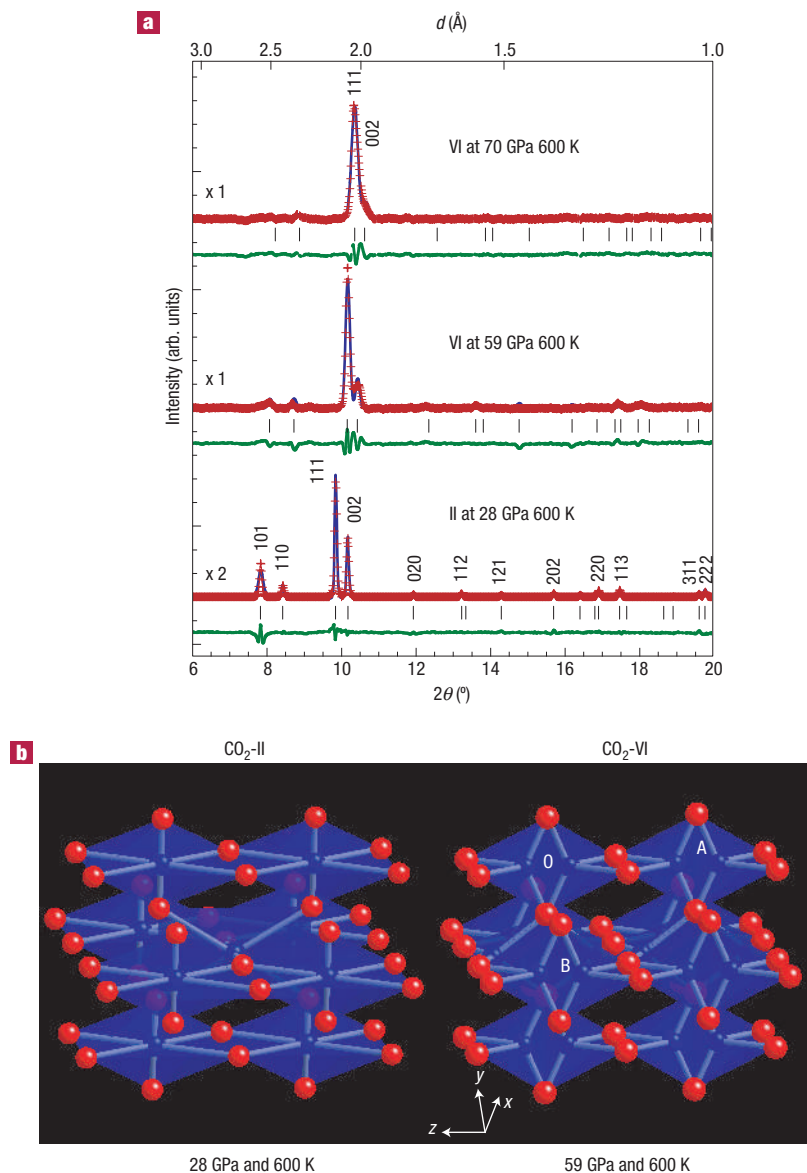


**Figure 5** Structural model for CO<sub>2</sub>-VI based on *in situ* X-ray diffraction measurements. **a**, ADXD patterns of CO<sub>2</sub>-II and VI (red plus symbols), shown together with the refined (blue lines) and difference (green lines) patterns. The X-ray wavelength was 0.3682  $\text{\AA}$ , and the  $hkl$  reflection lines are also marked. **b**, Crystal structures of phases II and VI in a stishovite-like  $P4_2/mnm$  structure. Note that carbon atoms in phase VI are disordered but maintain an average six-fold coordination within the carbon framework of  $sp^3$  hybridization.

presumably enhance their mutual solubility and chemical reactivity at the pressure–temperature conditions of the Earth's mantle. The structural instability of six-fold CO<sub>2</sub> at low pressures and its enhanced ionic character on decompression, would help account for the carbonate minerals originating from the Earth's interior<sup>21</sup> as well as for the high-temperature origin of carbonates in martian meteorites<sup>22</sup>.

## METHODS

Samples were loaded into an externally heated He gas mDAC by condensing 99.99% pure CO<sub>2</sub> gas at 10 MPa and 233 K in a sealed pressurized vessel. The use of resistively heated mDACs provided precise control over both pressure ( $\pm 2$  GPa up to 100 GPa) and temperature ( $\pm 10$  K up to 1,200 K). Furthermore, the mDAC applies a constant load by He gas to the sample during external

heating to 1,200 K at a given pressure, thus allowing isobaric heating experiments. Precise control over the experimental pressure–temperature path was crucial considering the significant metastability observed in CO<sub>2</sub> phases. The sample temperature was measured by a K-type thermocouple attached in close proximity to the diamond-anvil, and the pressure was determined by measuring the  $R_1$  luminescence of several micrometre-size rubies (Al<sub>2</sub>O<sub>3</sub>/Cr) placed around the sample. We carried out *in situ* Raman measurements using both 514.5 nm and 488.8 nm lines of an Ar<sup>+</sup> laser. For laser-heating experiments, we used the 1,054 nm line of a Nd:YLF laser to heat the CO<sub>2</sub> samples indirectly by heating either the ruby or the Re gasket edge as an absorber.

Angle-dispersive X-ray diffraction (ADXD) data were obtained at the microdiffraction beamline of the High Pressure Collaborative Access Team at the Advanced Photon Source by using focused ( $\sim 0.01$ – $0.02$  mm) monochromatic X-rays ( $\lambda = 0.3682 \text{\AA}$ ) and a high-resolution image plate detector. The recorded two-dimensional diffraction images (Debye–Scherrer's

rings) were then integrated to produce high-quality ADXD patterns using FIT2D and analysed with the XRDA and GSAS programs.

Received 12 October 2006; accepted 2 November 2006; published 10 December 2006.

## References

- Iota, V. & Yoo, C. S. Phase diagram of carbon dioxide: Evidence for a new associated phase. *Phys. Rev. Lett.* **86**, 5922–5925 (2001).
- Yoo, C. S. *et al.* Crystal structure of pseudo-six-fold carbon dioxide phase II at high pressures and temperatures. *Phys. Rev. B* **65**, 104103 (2002).
- Iota, V., Yoo, C. S. & Cynn, H. Quartzlike carbon dioxide: An optically nonlinear extended solid at high pressures and temperatures. *Science* **283**, 1510–1513 (1999).
- Sera, S., Corazon, C., Chiarotti, G. L., Scandolo, S. & Tossati, E. Pressure-induced solid carbonates from molecular CO<sub>2</sub> by computer simulation. *Science* **284**, 788–790 (1999).
- Yoo, C. S. *et al.* Crystal structure of carbon dioxide at high pressure: "Superhard" polymeric carbon dioxide. *Phys. Rev. Lett.* **83**, 5527–5530 (1999).
- Santoro, M. *et al.* Amorphous silica-like carbon dioxide. *Nature* **441**, 857–860 (2006).
- Aoki, K., Yamawaki, H., Sakashita, M., Gotoh, Y. & Takemura, K. Crystal structure of the high-pressure phase of solid CO<sub>2</sub>. *Science* **263**, 356–358 (1994).
- Olijnyk, H. & Jephcott, A. P. Vibrational studies on CO<sub>2</sub> up to 40 GPa by Raman spectroscopy at room temperature. *Phys. Rev. B* **57**, 879–888 (1998).
- Yoo, C. S., Iota, V. & Cynn, H. Nonlinear carbon dioxide at high pressures and temperatures. *Phys. Rev. Lett.* **86**, 444–447 (2001).
- Park, J.-H. *et al.* Crystal structure of bent carbon dioxide phase IV. *Phys. Rev. B* **68**, 014107 (2003).
- Gorelli, F. A., Giordano, V. M., Salvi, P. R. & Bini, R. Linear carbon dioxide in the high-pressure high-temperature crystalline phase IV. *Phys. Rev. Lett.* **93**, 205503 (2004).
- Kuchta, B. & Etters, R. Generalized free-energy method used to calculate the high-pressure, high-temperature phase transition in solid CO<sub>2</sub>. *Phys. Rev. B* **47**, 14691–14695 (1993).
- Sinclair, W. & Ringwood, A. E. Single crystal analysis of the structure of stishovite. *Nature* **272**, 714–715 (1978).
- Dong, J. *et al.* Investigation of hardness in tetrahedrally bonded nonmolecular CO<sub>2</sub> solids by density-functional theory. *Phys. Rev. B* **62**, 14685–14689 (2000).
- Holm, B., Ahuja, R., Belonoshko, A. & Johansson, B. Theoretical investigation of high pressure phases of carbon dioxide. *Phys. Rev. Lett.* **85**, 1258–1261 (2000).
- Hemley, R. J., Mao, H. K. & Chao, E. C. T. Raman spectrum of natural and synthetic stishovite. *Phys. Chem. Minerals* **13**, 285–290 (1986).
- Mammone, J. F., Nicol, M. & Sharma, S. K. Raman spectra of TiO<sub>2</sub>-II, TiO<sub>2</sub>-III, SnO<sub>2</sub>, and GeO<sub>2</sub> at high pressure. *J. Phys. Chem. Solids* **42**, 379 (1981).
- Yoo, C. S. in *Science and Technology of High Pressure* Vol. 1 (eds Manghnani, M. H., Nellis, W. J. & Nicol, M. F.) 86–89 (Univ. Press, Hyderabad, India, 2000).
- Tassone, F., Chiarotti, G. L., Rousseau, R., Scandolo, S. & Tosatti, E. Dimerization of CO<sub>2</sub> at high pressure and temperature. *ChemPhysChem* **6**, 1752–1756 (2005).
- Cohen, R. E. in *High Pressure Research: Application to Earth and Planetary Sciences* (eds Syono, Y. & Manghnani, M. H.) 425 (Terra Scientific, AGU, Washington DC, 1992).
- Santillan, J. & Williams, Q. A high-pressure infrared and X-ray study of FeCO<sub>3</sub> and MnCO<sub>3</sub>: comparison with CaMg(CO<sub>3</sub>)<sub>2</sub>-dolomite. *Phys. Earth Planet. Inter.* **143/144**, 291–304 (2004).
- Harvey, R. P. & McSween, H. Y. A possible high-temperature origin for the carbonates in the martian meteorite ALH84001. *Nature* **382**, 49–51 (1996).

## Acknowledgements

The work has been supported by the LDRD and PDRP programs at the LLNL, University of California, under the auspices of the US-DOE under contract number W-7405-ENG-48. The X-ray work was done by using the High Pressure Collaborating Access Team's micro-diffraction beamline (16IDB) of the Advanced Photon Source. Use of the HPCAT facility was supported by DOE-BES, DOE-NSNSA (CDAC, LLNL, UNIV), NSF, DOD-TACOM and the W.M. Keck Foundation. Correspondence and requests for materials should be addressed to V.I. or C.-S.Y. Supplementary Information accompanies this paper on [www.nature.com/naturematerials](http://www.nature.com/naturematerials).

## Author contributions

Project planning: V.I., C.S.Y., samples and Raman measurements: V.I., Z.J., XRD measurements: V.I., C.S.Y., W.E., H.C., data analysis: V.I., C.S.Y., J.H.K.

## Competing financial interests

The authors declare that they have no competing financial interests.

Reprints and permission information is available online at <http://npg.nature.com/reprintsandpermissions/>